water

MDPI

Article

Enhancing Flood Inundation Simulation Under Rapid Urbanisation and Data Scarcity: The Case of the Lower Prek Thnot River Basin, Cambodia

Takuto Kumagae, Monin Nong, Toru Konishi, Hideo Amaguchi and Yoshiyuki Imamura *

Department of Civil and Environmental Engineering, Graduate School of Urban Environmental Sciences, Tokyo Metropolitan University, Hachioji City 192-0397, Japan; kumagae-takuto@ed.tmu.ac.jp (T.K.); monin@cdri.org.kh (M.N.); trkonishi2022@icloud.com (T.K.); amaguchi@tmu.ac.jp (H.A.)
* Correspondence: imamura@tmu.ac.jp

Abstract

Flooding poses a major hazard to rapidly urbanising cities in Southeast Asia, and risks are projected to intensify under climate change. Accurate risk assessment, however, is hindered by scarcity of hydrological and topographic data. Focusing on the Lower Prek Thnot River Basin, a peri-urban catchment of Phnom Penh, Cambodia, the study applied the Rainfall–Runoff–Inundation model and systematically augmented inputs: hourly satellite rainfall data, field-surveyed river cross-sections and representation of hydraulic infrastructure such as weirs and pumping. Validation used Sentinel-1 SAR-derived flood-extent maps for the October 2020 event. Scenario comparison shows that rainfall input and channel geometry act synergistically: omitting either degrades performance and spatial realism. The best configuration (Sim. 5) Accuracy = 0.891, Hit Ratio = 0.546 and True Ratio = 0.701 against Sentinel-1, and reproduced inundation upstream of weirs while reducing overestimation in urban districts through pumping emulation. At the study's 500 m grid, updating land use from 2002 to 2020 had only a minor effect relative to rainfall, geometry and infrastructure. The results demonstrate that targeted data augmentation—combining satellite products, field surveys and operational infrastructure—can deliver robust inundation maps under data scarcity, supporting hazard mapping and resilience-oriented flood management in rapidly urbanising basins.

Keywords: Lower Prek Thnot River Basin; Phnom Penh; Cambodia; flood modelling; RRI model; data scarcity; remote sensing; satellite rainfall; urbanisation

check for updates

Academic Editors: Akhilesh Surjan and Mikio Ishiwatari

Received: 24 September 2025
Revised: 28 October 2025
Accepted: 30 October 2025
Published: 11 November 2025

Citation: Kumagae, T.; Nong, M.; Konishi, T.; Amaguchi, H.; Imamura, Y. Enhancing Flood Inundation Simulation Under Rapid Urbanisation and Data Scarcity: The Case of the Lower Prek Thnot River Basin, Cambodia. *Water* **2025**, *17*, 3222. https://doi.org/10.3390/w17223222

Copyright: © 2025 by the authors. Licensee MDPI, Basel, Switzerland. This article is an open access article distributed under the terms and conditions of the Creative Commons Attribution (CC BY) license (https://creativecommons.org/licenses/by/4.0/).

1. Introduction

Flooding is one of the most frequent and damaging natural disasters worldwide. It accounts for 44% of all reported disasters over the past two decades [1]. Its severity has been magnified by anthropogenic factors, including land-use change, urbanisation, and climate change [2].

Southeast Asia faces multiple challenges—climate change, rapid urbanisation and population growth—that render it highly vulnerable to hydro-climatic hazards for sustainable economic development. Climate change would intensify the hydrological cycle, thereby amplifying the frequency and severity of extreme precipitation and flood hazard and damages across the region [3–5]. These changes are compounded by rapid population growth [6], which increases exposure to natural hazards and places additional stress on

already fragile infrastructures. Consequently, flooding has become one of the most pressing threats to sustainable development in many Southeast Asian countries [7].

Despite the severity of the problem, the body of literature on flood risks in Southeast Asia remains uneven. Considerable progress has been made in relatively data-rich countries such as Thailand and Vietnam, where extensive hydrological and hydraulic models have been developed for major river basins, including Chao Phraya and Mekong [8–10]. In contrast, Cambodia—despite its high exposure to seasonal flooding—has received far less research attention, primarily due to the scarcity of reliable hydrological, meteorological and topographic data [11,12]. Ground-based monitoring networks remain sparse, river channel cross-section surveys are infrequent, and rainfall records are often incomplete. These limitations hinder the calibration and validation of flood models, particularly at the urban and peri-urban scale. Against this backdrop, several studies have attempted to assess flood risks under data-scarce conditions by employing qualitative analyses, conducting simulations with low spatial or temporal resolution, or focusing on limited datasets restricted to small urban areas such as Phnom Penh's city centre. Below, existing research on Cambodia and the peri-urban areas of Phnom Penh is reviewed.

Hydrological and climate-related flood risks in Cambodia have been widely studied, yet urban-scale modelling remains limited. Basin-wide models have explored the influence of development and climate change on discharge [13], while remote-sensing analyses (MODIS data) have detected broad inundation patterns [14–16]. Urban-scale studies have documented rapid land-use change and its implications for flood exposure—Phnom Penh's urban expansion has expanded more than eightfold since the 1970s, replacing wetlands and natural retention zones [15,17–19]. While these studies show spatial trends, they lack quantitative runoff modelling.

Social and institutional inequality further compounds the physical risks. Inequitable access to infrastructure, tenure insecurity and inadequate drainage facilities exacerbate vulnerability, particularly in informal settlements [20–22]. Consequently, areas experiencing the most dynamic land-use change and hydrological transformation have heightened flood susceptibility in districts such as Dangkao and Mean Chey, which now host major residential, industrial and infrastructure projects. Yet, these peri-urban zones remain underrepresented in flood modelling compared with the city centre.

Previous flood studies in Phnom Penh illustrate both progress and limitations in modelling resolution and data integration. Kudo et al. (2016) applied the Rainfall–Runoff–Inundation (RRI) model to the Lower Mekong River Basin, including Phnom Penh [23]. However, its 2 km spatial resolution was too coarse for city-level analysis. In contrast, Heng et al. (2021) addressed this by employing a high-resolution flood analysis using the FLO-2D model [24]. They utilised surveyed DEM data points and rainfall data independently collected between 2009 and 2016. The model operated at a 10-metre resolution and incorporated the effects of climate change. However, their study area was limited to 12.5 km^2 within the city centre. This area is more elevated than the surrounding regions and, therefore, less susceptible to fluvial flooding. These studies demonstrate the trade-off between spatial coverage and model resolution that characterises flood modelling under data constraints. More recently, Phy et al. (2022) modelled floods in the Lower Prek Thnot River Basin (LPTRB) using the RRI model [25]. It is considered a peri-urban area undergoing rapid urbanisation. They used the RRI model to assess the potential impacts of climate change. To compensate for the lack of local data, they relied on various satellite-based sources, including the Multi-Error-Removed-Improved Terrain (MERIT) DEM for topographical data, Google Earth imagery for estimating river widths and Global Precipitation Measurement (GPM) data for rainfall input. While innovative, their approach relied on outdated land-use data (from 2002) to simulate a 2020 event and

rainfall inputs at daily resolution likely miss short-term flood peaks. These limitations highlight the difficulty of capturing rapid environmental and urban transitions using static or low-frequency datasets.

The urgency of applying such methods may be further warranted by Phnom Penh's evolving socio-environmental context. Climate change is likely to influence regional hydrological regimes [15,17]. At the same time, Phnom Penh and its surroundings appear to be undergoing rapid urbanisation, outpacing the speed of provision of proper flood-control infrastructure. These dynamics are considered to exacerbate existing socio-economic inequalities [19,21,22], as the urban poor are thought to be disproportionately exposed to flood risks and less able to recover from impacts.

Research Objectives: This study aims to enhance flood inundation modelling in the LPTRB by integrating multi-source datasets—satellite-derived, ground-based and field-surveyed—within a unified modelling framework. Specifically, it develops a data-augmentation scheme for the RRI model that progressively incorporates (i) hourly bias-corrected satellite rainfall, (ii) field-surveyed river channel cross-sections, and (iii) hydraulic infrastructure (weirs and pumping). The study evaluates how data augmentation influences the performance and reliability of RRI-based flood simulations. It quantifies the relative contributions of rainfall resolution, channel geometry, land-use update and drainage operations to model performance. Methodologically, this research contributes to the growing body of flood modelling under data scarcity by demonstrating how remote sensing and targeted field surveys can be combined to improve hydrodynamic reliability. Practically, the findings support hazard mapping and adaptive flood management in Phnom Penh's peri-urban districts—areas undergoing rapid land transformation yet lacking reliable monitoring data. By focusing on the LPTRB, the study also underscores the importance of extending flood risk assessment beyond dense city centres to transitional zones where exposure is accelerating.

2. Materials and Methods

2.1. Study Area

Phnom Penh, Cambodia's capital, lies at the confluence of the Mekong, Tonle Sap and Bassac Rivers, with its southern periphery intersected by the Prek Thnot River. Over the past two decades, rapid urban growth has led to extensive reclamation of wetlands, severely diminishing natural flood retention capacity [26]. These peri-urban areas are among the fastest developing zones, yet they are underrepresented in flood risk research.

This study targeted the Prek Thnot River, the only tributary of the Bassac (Mekong system) flowing through Phnom Penh thus is hydrologically the most critical for flood in Phnom Penh.

The climate in this region is characterised by tropical monsoons. Based on rainfall observation (Pochentong) in Phnom Penh from 1981 to 2021, the mean annual precipitation was 1416 mm, with a standard deviation of 236 mm, resulting in a coefficient of validation of 16.7%. Approximately 80–85% of the annual precipitation occurred between May and October, corresponding to the wet season. During the wet season, the mean monthly precipitation ranged from 120 to 270 mm, and the monthly standard deviation was as high as 80–90 mm, indicating pronounced interannual variations in rainfall intensity and duration. In contrast, precipitation during the dry season from November to April was remarkably low, averaging less than 30 mm per month. In terms of temperature, according to the ERA5 reanalysis products for 1991–2020, the annual mean temperature remains high, generally ranging from 27 °C to 30 °C. The highest temperatures occur in March and April, when the average maximum temperature reaches approximately 37 °C [27].

The Prek Thnot catchment is divided into upper and lower basins and has a total area of approximately 6106 km^2. The lower section, which is defined by the Peam Khley discharge and water level station as its inlet, constitutes the study area, hereafter referred to as the LPTRB (Figure 1). The LPTRB covers approximately 2389 km^2, and the main river channel length within the LPTRB is approximately 192 km. The LPTRB fully or partially includes Phnom Penh's southern districts: Kamboul, Pou Senchey, Dangkao, and Mean Chey. These peri-urban districts have experienced rapid in-migration and land conversion in recent decades. The LPTRB districts have also undergone sharp population growth, underscoring their importance for flood risk assessment. Across the four districts, residents increased as follows: Dangkao nearly doubled, rising from 81,700 in 2005 to 145,600 in 2022 (+78%). Mean Chey grew more modestly, from 162,700 to 190,600 (+17%) over the same period. Pou Senchey reached 233,400 in 2022, rising 26% since 2015. Kamboul, though smaller, grew from 52,300 in 2019 to 69,100 in 2022 (+32%) [28]. Omitting these districts from flood modelling would underestimate citywide flood exposure, since risk has shifted beyond the urban core.

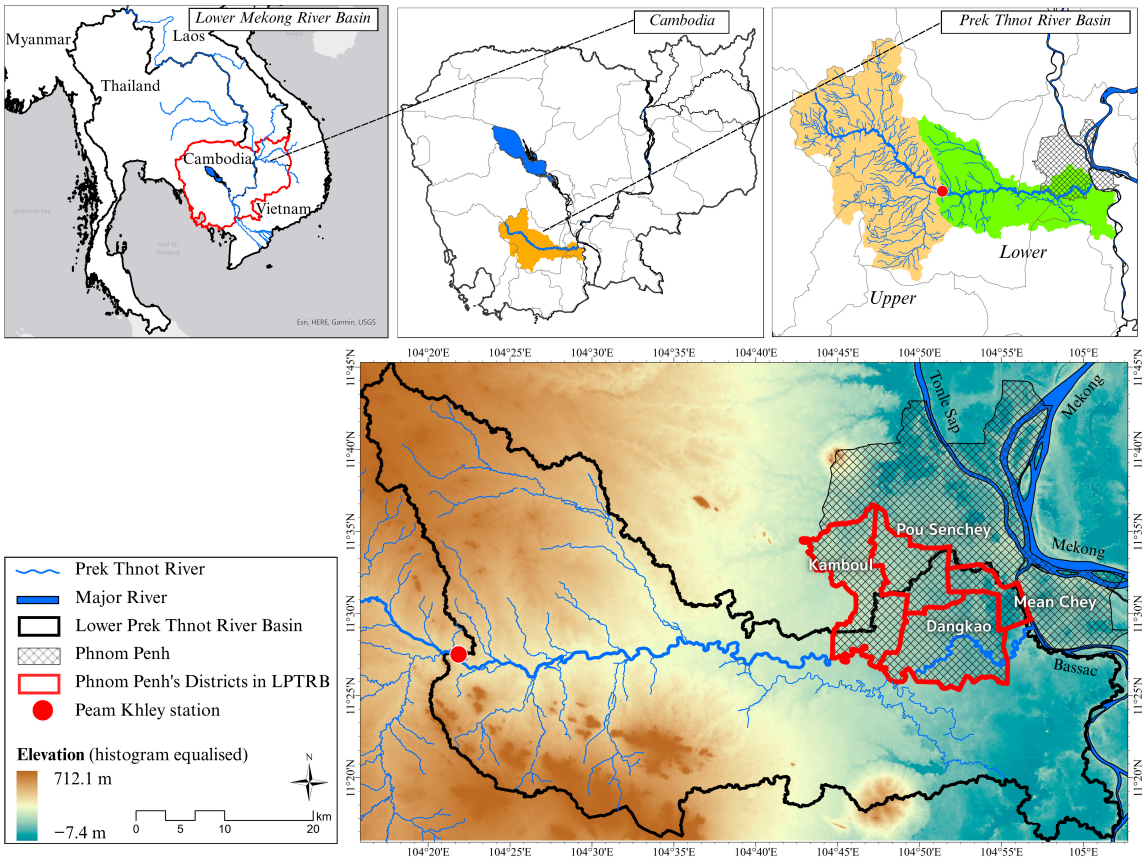


Figure 1. Overview of the Lower Prek Thnot River Basin.

The LPTRB is undergoing rapid urban development. A prominent example is Techo International Airport, the new airport for Phnom Penh, scheduled to open in September 2025. It is being constructed on reclaimed wetland areas, specifically the Boeung Cheung Loung Lake in Kandal Province. The airport will span approximately 26 km^2 and is projected to be the ninth largest in the world [29,30]. Industrial parks and special economic zones are also expanding in Dangkao and Mean Chey. The 26 km^2 ING City project, a satellite city development in southern Phnom Penh led by ING Holdings, exemplifies this transformation, replacing lakes that previously absorbed nearly 80% of urban wastewater and runoff. This concentration of people and assets in flood-prone peri-urban areas

highlights the need for accurate flood risk estimation. Accurate estimation of flood risk in these peri-urban districts would equip local and national authorities to design preventive measures and strengthen preparedness strategies. Improved modelling will provide evidence for authorities to strengthen preparedness, guide urban planning, and prioritise flood-control investments.

Urban planning regulations have not kept pace with these transformations. The Phnom Penh City Land Use Master Plan 2035 designated southern Dangkao as an "Area Needing Further Study" [31]. Although Boeung Tompun and Boeung Cheung Aek Lakes were classified as conservation zones, these designations failed to prevent degradation. Investment proposals diverging from the master plan may still be approved if deemed to offer significant economic potential. These regulatory gaps, coupled with rapid growth, highlight the LPTRB's importance for flood risk assessment under data scarcity and urbanisation. (General Directorate of Land Management and Urban Planning, interview by authors, 25 March 2025).

2.2. Model Framework

To address data scarcity, satellite data were extensively utilised for input datasets, except for river channel cross-sectional data. The cross-section data were acquired through a field survey conducted by the authors in March 2025. For bias correction, rainfall gauges, water level and discharge data, which are of lower temporal and spatial resolution compared to satellite data, were obtained from the Ministry of Water Resources and Meteorology (MOWRAM), Cambodia. Using these variables, a two-dimensional flood model was generated with the RRI Model to obtain the probable flood depth and extent for the target event. The resulting flood extent maps were subsequently calibrated using historical flood extent maps derived from Synthetic Aperture Radar (SAR) imagery. A schematic diagram of the procedure is presented in Figure 2.

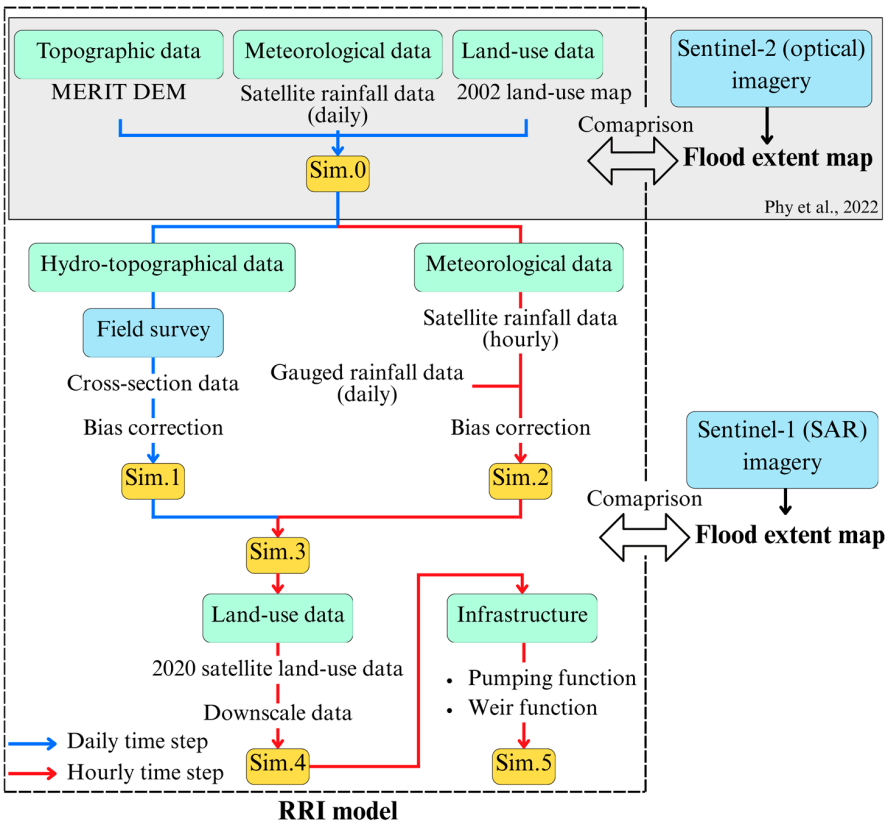


Figure 2. Model Framework. Sim. 0 and Sentinel-2 (optical) imagery (Phy et al., 2022) [25].

2.3. RRI Model

The RRI model (Ver. 1.4.2), utilised in this study, is a two-dimensional model that is capable of simulating rainfall–runoff and flood inundation simultaneously (Figure 3) [8,32]. The model equations are derived based on the mass balance equation (Equation (1)) and momentum equations (Equations (2) and (3)).

$$\frac{\partial h}{\partial t} + \frac{\partial q_x}{\partial x} + \frac{\partial q_y}{\partial y} = r - f \tag{1}$$

$$\frac{\partial q_x}{\partial t} + \frac{\partial u q_x}{\partial x} + \frac{\partial v q_x}{\partial y} = -gh\frac{\partial H}{\partial x} - \frac{\tau_x}{\rho_w} \tag{2}$$

$$\frac{\partial q_y}{\partial t} + \frac{\partial u q_y}{\partial x} + \frac{\partial v q_y}{\partial y} = -gh\frac{\partial H}{\partial y} - \frac{\tau_y}{\rho_w} \tag{3}$$

where h is the height of water from the local surface, q_x and q_y are the unit width discharges in x and y directions, u and v are the flow velocities in x and y directions, r is the rainfall intensity, f is the infiltration rate, H is the height of water from the datum, ρ_w is the density of water, g is the gravitational acceleration, and τ_x and τ_y are the shear stresses in x and y directions.

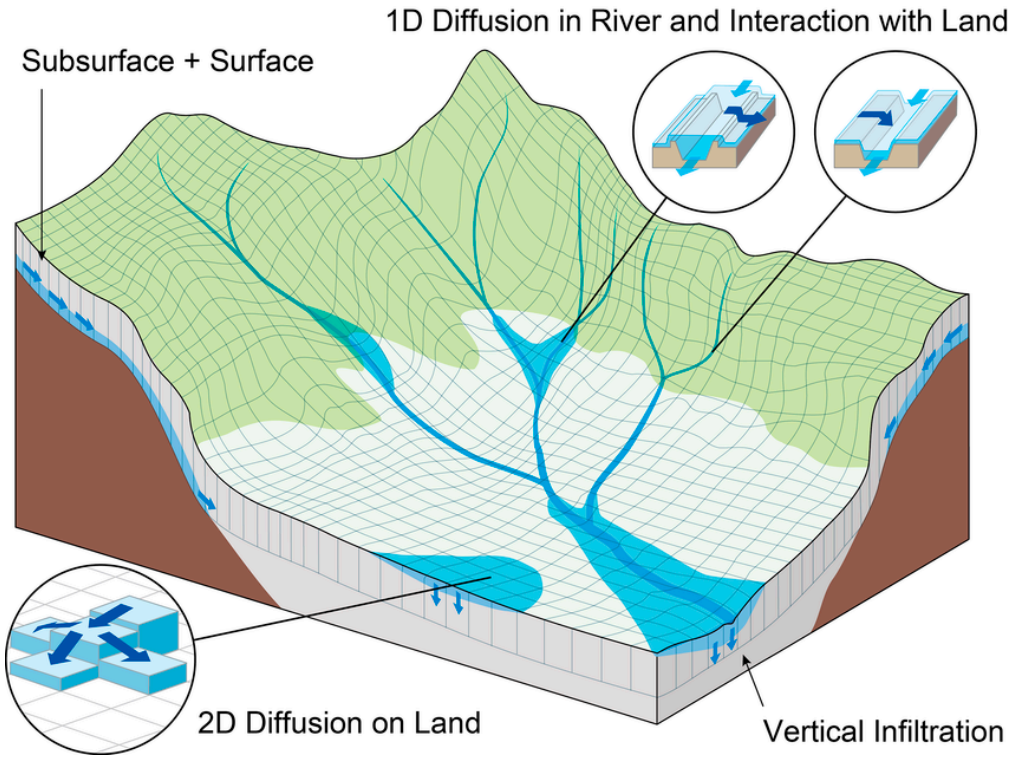


Figure 3. Structure of RRI model (reproduced from Sayama et al., 2015 [8], © Authors 2015. Licensed under CC BY 3.0.).

A one-dimensional diffusive wave model is applied to river grid cells (Equations (4) and (5)). The geometry is assumed to be rectangle, whose shapes are defined by width W, depth D and embankment height H_e. When detailed geometry information is not available, the width and depth are approximated by the following function of upstream contributing area A [km^2].

$$W = C_w A^{S_w} \tag{4}$$

$$D = C_D A^{S_D} \tag{5}$$

where C_w, S_w, C_D and S_D are geometry parameters.

The RRI model is widely utilised, primarily in data-scarce regions, particularly across Southeast Asia. As Kakinuma (2022) [33] highlights, projects by the Japan International Cooperation Agency (JICA) and the Ministry of Education, Culture, Sports, Science and Technology (MEXT) have implemented the RRI model in basins such as the Chao Phraya River Basin (Thailand), Indus River Basin (Pakistan), Pampanga River Basin (Philippines), Solo River Basin (Indonesia), Lower Mekong River Basin (Cambodia) and Kelantan River Basin (Malaysia) [33]. These examples typically involve larger catchment areas ranging from 10,434 km^2 to 160,000 km^2 compared to the LPTRB. However, progress is also evident in implementing the RRI model in small to medium-sized rivers. For instance, the Public Works Research Institute (PWRI) in Japan, also cited by Kakinuma (2022) [33], has applied it to the Kagetsu River Basin (136 km^2). Despite these applications in medium-sized or smaller river basins, it is crucial to strike a balance between data availability and computational grid size.

Building on these capabilities, in this study, a computational grid size of 500 m was adopted following Phy et al. (2022) [25], which balances consistency with input resolutions (GSMaP rainfall 10 km, MERIT DEM 90 m, Landsat land use 30 m) and computational efficiency. The low-relief terrain of the LPTRB favours shallow overland propagation, and because the RRI model couples a 1-D river network to a 2-D floodplain, results are relatively insensitive to finer mesh sizes for basin-scale routing; 500 m was therefore deemed sufficient to capture the dominant hydraulics without instability, while allowing explicit representation of key structures (weirs, pumping stations) at the cell scale. The parameters used in this model, referred to Phy et al. (2022), are shown in Table 1 [25].

Table 1. Values of each parameter set in the RRI model in the study.

	Land Use				
Parameter	**Forest**	**Urban**	**Water Body**	**Wetland**	**Agriculture**
n_{river}			0.03		
n_{slope}	0.20	0.05	0.05	0.03	0.01
d	0.60	0.00	0.80	0.00	0.40
ϕ_a	0.40	0.30	0.30	0.30	0.30
k_v	—	—	—	1.66×10^{-7}	1.66×10^{-7}
S_f	—	—	—	0.273	0.273
k_a	0.10	—	0.10	—	—
ϕ_m	—	—	0.05	—	—

Notes: n_{river} and n_{slope} = Manning's coefficient for river and slope (m $^{-1/3}$ s); d = soil depth (m); S_f = wetting front soil suction head; k_v = vertical hydraulic conductivity (m /s); k_a = lateral saturated hydraulic conductivity (m /s); ϕ_a = soil porosity; and ϕ_m = unsaturated porosity.

Hydrological data were acquired from the MOWRAM. Daily water level and discharge observed at the Prek Thnot River's Pream Khley station (104°350′ E, 11°461′ N) were applied as input for the model's boundary conditions. Topological data: Digital Elevation Model (DEM) with approximately 90-m resolution, flow direction (DIR), and flow accumulation (ACC) were obtained from the MERIT DEM [34]. The original DEM data was downscaled to a 500 m mesh. From the resampled DEM, DIR and ACC were derived to delineate the RRI drainage network and overland flow pathways. This resolution balances basin-scale routing needs with numerical stability but inevitably smooths micro-topography in reclaimed/urban areas; these implications are considered when interpreting shallow ponding.

2.4. Target Event

The target event period was defined as 7 October to 26 October 2020. This event was selected because rainfall gauge records are largely unavailable prior to 2015: of the 10 stations, 9 located outside Phnom Penh either contain substantial gaps or no data at all. Since this study applies bias correction of satellite rainfall using observed records, only flood events after 2015 could be considered. The 2020 event featured Phnom Penh's heaviest consecutive rainfall in the first two decades of this century, with 401 mm recorded over 20 days at the Pochentong station. As of 26 October, approximately 5587 households in Phnom Penh were reported to be affected by flooding [35].

3. Data Augmentation

3.1. Meteorological Data

This study utilised hourly satellite data for input data and daily rainfall observed at gauges acquired from the MOWRAM for the bias correction. Hourly rainfall data from the GSMaP_MVK (ver. 7.3112.0) acquired from the Global Precipitation Measurement (GPM) under the joint mission between JAXA and NASA at the resolution of approximately 10 × 10 km was incorporated (Figure 4). Although the GSMaP has the world's highest spatiotemporal resolution, a comparison with radar observations in Vietnam revealed that it tended to estimate high-intensity rainfall less frequently, reaching a ceiling of around 15 mm/h [36]. Empirically, a comparison between the daily rainfall data from 10 rainfall gauges and the corresponding GSMaP grid data, encompassing those gauges, revealed that the total rainfall amount during the period was 0.88 to 3.69 times larger (Figure 5). To bring the total amount of GSMaP rainfall into agreement with the observed precipitation, the RESTEC method (Tsuda, 2016) was employed for correction (Equations (6)–(8)) [37]. Specifically, the correction was conducted using the Inverse Distance Weighting (IDW), leveraging data from 34 GSMaP grids that cover the basin and from 10 rainfall gauges.

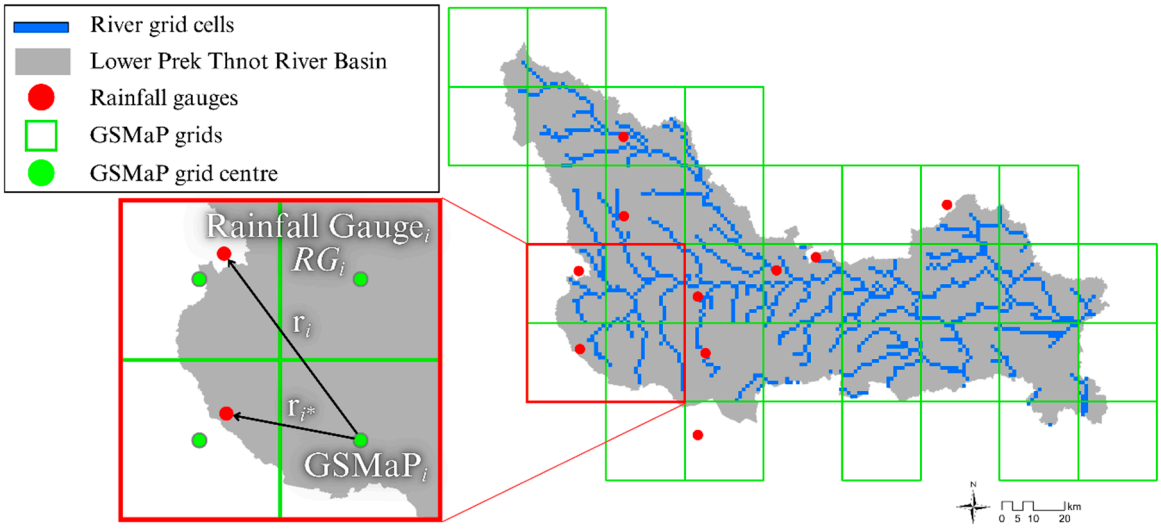


Figure 4. Spatial distribution of rainfall gauges and GSMaP grids in the Lower Prek Thnot River Basin.

$$CF_i = RG_i / GSMaP_i \tag{6}$$

$$CF_{GSma\ PGrid} = \frac{\sum \frac{CF_i}{r_i}}{\sum \frac{1}{r_i}} \tag{7}$$

$$RAIN_{GSMaP\ Grid} = GSMaP \times CF_{GSmaP\ Grid} \tag{8}$$

where CF_is are correction factors, RG_is are observed rainfall at each gauge, $GSMaP_i$s are satellite rainfall at each GSMaP grid, r_is are distance between the centre of GSMaP grid and reference rainfall gauges and $RAIN_{GSMaP\ Grid}$s are the corrected satellite rainfall at each GSMaP grid.

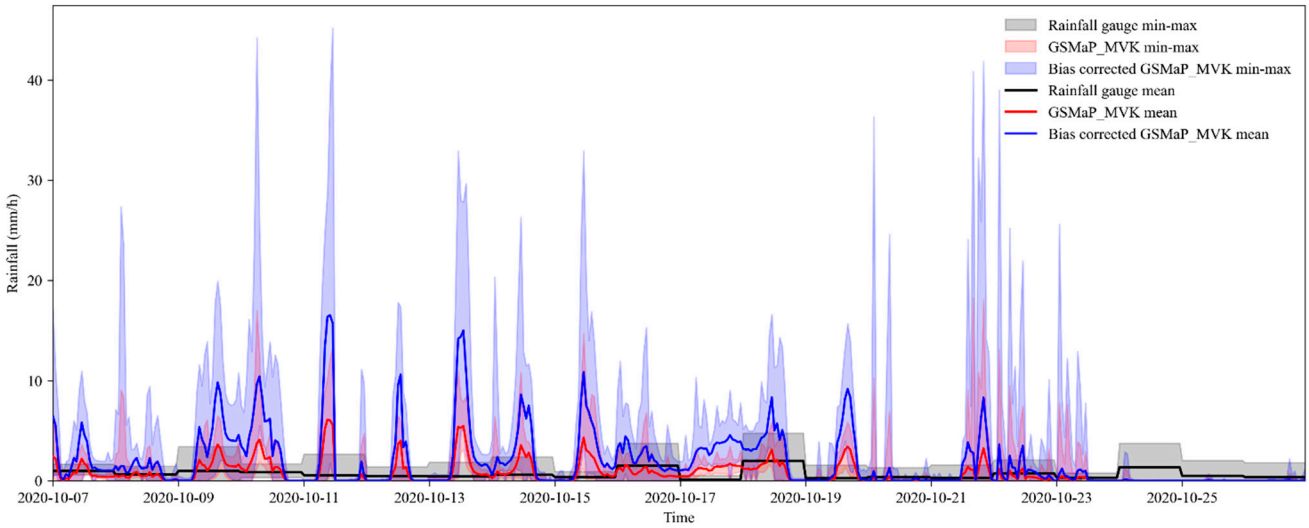


Figure 5. Temporal comparison of observed and GSMaP rainfall data.

3.2. Land Use Data

The most recent accessible land use data from authorised organisations remains based on the Mekong River Commission's 2002 dataset, which has been utilised in the previous study [25] for flood inundation analyses. For this study, the global 2000–2020 land cover and land use change dataset, derived from the Landsat archives [38], was subsequently employed. Landsat data are notable as the sole satellite data record that enables multi-decadal land cover assessment at a medium spatial resolution of 30 m per pixel [39]. This dataset was also downscaled to a 500 m mesh and reclassified to five categories—Forest, Urban, Agriculture, Water body, Wetland—following the Mekong River Commission scheme. Class-specific hydraulic and soil parameters were assigned as in Table 1. Comparison of land use distribution in the study area between 2002 and 2020 is indicated in Figure 6 and Table 2. These indicates pronounced urban expansion and agricultural contraction between 2002 and 2020, together with localised wetland losses near peri-urban districts. The Urban share increased from ~0.8% (2002) to ~17.0% (2020), while Agriculture and Forest decreased by ~10.5 and 6.9 percentage points, respectively; Wetlands approximately doubled in relative area (~1.4% → 2.7%), though their absolute extent remains limited, and Water bodies changed little. The 2020 land-use layer is used in Sim. 4 (and retained in Sim. 5) to assess the incremental effect of contemporary land-surface conditions within the data-augmentation framework.

Table 2. Land use transition between 2002 and 2020 over the Lower Prek Thnot River Basin.

	Land Use				
Year	**Forest**	**Urban**	**Water Body**	**Wetland**	**Agriculture**
2002	478.3	15.5	37.8	28.5	1475.8
2020	337.0	345.8	36.5	54.3	1262.3

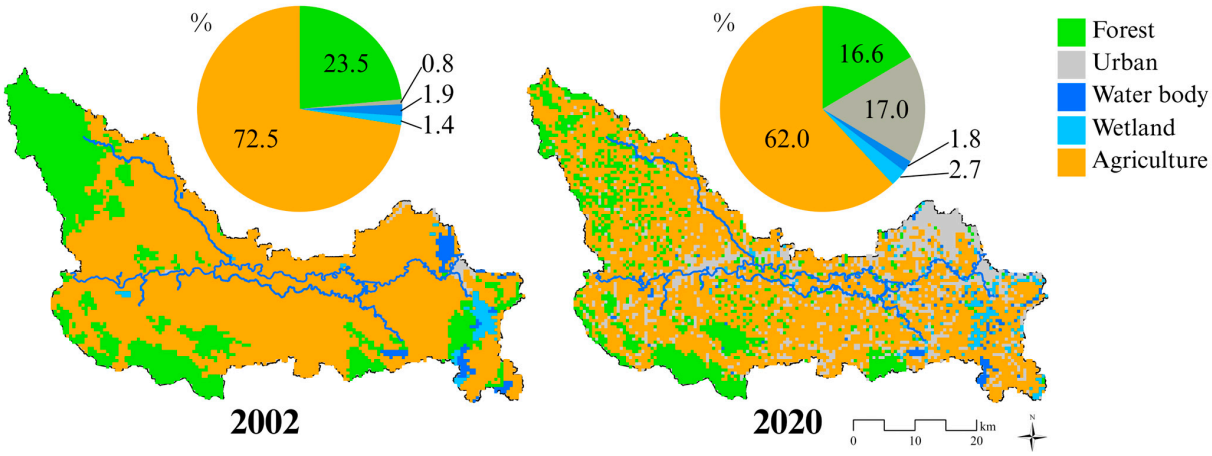


Figure 6. Spatial transition of land use between 2002 and 2020 over the Lower Prek Thnot River Basin.

3.3. River Channel Cross-Section

River channel cross-sections were acquired through field surveys conducted by Takuto Kumagae, Monin Nong, and Hideo Amaguchi from 16 to 22 March 2025. As no channel cross-section data were available for the study area, the survey was carried out to obtain the general geometry of the river sections (Figure 7a). Particular emphasis was placed on the downstream region, where inundation areas are extensive and population and assets are concentrated; hence, intensive measurements were conducted in this area. In addition to six sites along the main river, six sites on major downstream tributaries were also surveyed. For terrestrial measurements, a portable Global Navigation Satellite System (GNSS) receiver, specifically the Drogger by BizStation Corp., was employed (Figure 7b). Underwater measurements were conducted using a GPS-equipped Sound Navigation Ranging (SONAR) device, the DEEPER by Friday Lab (Figure 7c). The GNSS base station was installed on the rooftop of a six-storey building in Phnom Penh, selected because no taller structures were located nearby (Figure 7). Regarding geodetic referencing, corrections were applied using the elevation of one weir specified in a JICA report [40] and the elevations of two distinct points marked on local embankments (Figure 7e).

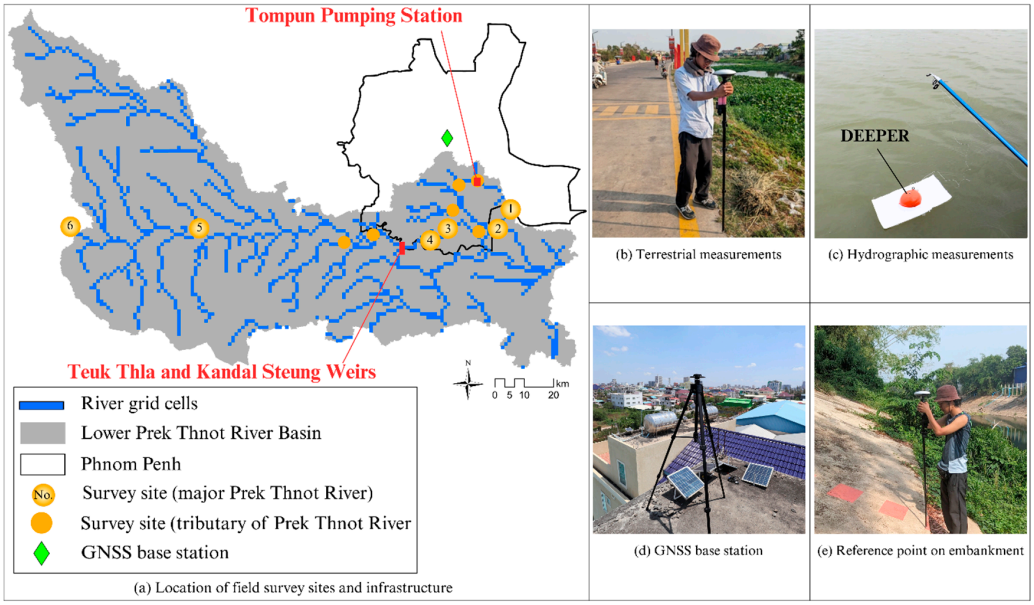
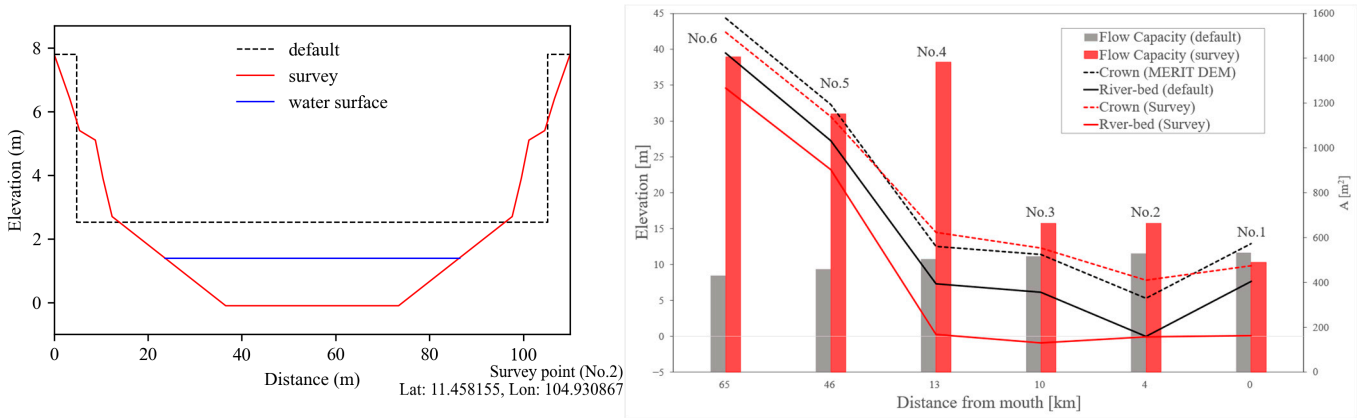


Figure 7. Overview of field survey; (**a**) location of field survey sites and infrastructure; (**b**–**e**) photographs from field survey.

Data from six locations on the main river and another six locations on its tributaries were processed and formatted for the use in the 1-D river network of the RRI model as representative cross-sections. Where surveyed data were available, they replaced the default cross-section areas (A [m^2]) calculated by Equations (4) and (5) using ACC; in other reaches, the default geometry was retained. The field survey's results revealed that the actual cross-section areas were bigger in the overall trend, particularly significant in the upstream (Figure 8). This data was incorporated into Sim. 1 and subsequent simulations, representing a key improvement in channel conveyance capacity within the data augmentation sequence.



(**a**) (**b**)

Figure 8. Distance from the outlet and corresponding channel characteristics along the main Prek Thnot River; (**a**) Example of comparison between default and observed channel cross-sections; (**b**) Comparison of default and observed channel cross-sections, and channel geometry.

3.4. Hydraulic Infrastructure

The basin features two movable weirs, Teuk Thla Weir and Kandal Steung Weir, both of which effectively function as dams at a single point. The standard RRI model only allows for dam capacity and constant discharge configurations. When the capacity is exceeded, the entire inflow is discharged, which is not suitable for these specific structures. Therefore, after confirmation from the MOWRAM documents that the dams were fully open during the event, their respective river channel cross-sections were adjusted. This adjustment reflected a cross-sectional area of 345 m^2, corresponding to the fully open state.

The Tompun Pumping Station is designed to drain urban runoff into Boeung Cheng Aek Lake and its surrounding suburban areas, with a design discharge of 15 m^3/s for its inlet channel. As RRI model (Version 1.4.2) does not support pump simulation, pumping was reproduced by specifying both the drainage volume from the lowland area and the inflow volume to the river channel. Drainage from the lowland area was represented by assigning an equivalent amount of evapotranspiration [41]. Inflow to the river was represented by setting the discharge of the land cell immediately downstream of the pump station as a boundary condition [42].

These hydraulic components, introduced in Sim. 5, allow the model to explicitly represent urban drainage operations, thereby improving inundation accuracy in the central and downstream LPTRB areas.

3.5. SAR Imagery

Since no spatial records were available for the 2020 flood event, SAR imagery was utilised to identify inundated areas. SAR data is ideal for flood detection because it can penetrate clouds and atmospheric interference, which are common during flooding events,

and it can be used at night since it doesn't rely on spectral reflectance from the Earth's surface. Water surfaces can be reliably classified by applying the backscatter coefficient. Building on this principle, Iida et al. proposed a flood monitoring approach using SAR imagery, validating the brightness difference method by comparing pre-flood and during-flood SAR images [43]. A study comparing the performance and suitability of various SAR datasets against the hydraulic inundation model (HEC-RAS) in the Lower Mekong River Basin recommended applying a −15 dB threshold for optimal water surface detection when using Sentinel-1 imagery, as it demonstrated the highest agreement with the model-simulated flood extent [44].

Accordingly, Sentinel-1 images acquired on 23 October 2020 (during-flood) and 25 July 2020 (pre-flood) were obtained via Google Earth Engine. These dates were selected based on the confirmation of significant rainfall events recorded at the Pochentong gauge in Phnom Penh after July 25. Water surfaces were then extracted from both datasets, and their differences were used to estimate the inundated area. This analysis was used to generate a historical flood extent map representing the 2020 event.

Figure 9 compares a flood map derived from Sentinel-2 imagery used in the previous study with the estimated inundation extent generated using Sentinel-1 data in this study. Sentinel-1 was used based on limitations observed in the Sentinel-2 flood map, which, as an optical satellite product, exhibited discontinuous inundation patterns in elevated areas. To address this, the present study employed Sentinel-1, a Synthetic Aperture Radar (SAR) satellite, which is not affected by cloud cover and can capture surface conditions regardless of lighting. Given the spatial resolution of Sentinel-1 (10 m), areas were extracted and downscaled if more than 10% of the 500 m computational grid cells were detected as inundated. However, SAR data has inherent limitations. In urban and forested areas, where the ground surface is often obscured, it is difficult to accurately detect inundation using SAR data alone. Due to the presence of floating vegetation, such as morning glory, much of the water surface of Boeung Cheung Aek Lake (Figure 10) in Phnom Penh could not be detected by Sentinel-1 SAR imagery during the flood event. These floating plants rise with the water level and obscure the underlying water surface, limiting the sensor's ability to capture inundation accurately. As the lake plays a key role in draining rainfall runoff, the entire area was treated as inundated in this study.

Figure 11 presents the terrain and the areas identified as inundated by both Sentinel-2 and Sentinel-1 (SAR) imagery as an illustrative example. The region shown is characterised by low-lying areas along the river channel, with relatively higher elevations located beyond these floodplains. Sentinel-2 imagery indicates inundation across wide portions of the higher-elevation areas, despite the absence of flooding in the adjacent low-lying floodplains. In contrast, Sentinel-1 imagery detects considerably fewer inundated areas in the higher-elevation areas while capturing a relatively larger extent of inundation along the river channel. These findings suggest that inundation detection by Sentinel-1 imagery provides more reliable results.

3.6. Data Limitations and Assumptions

The simulations were constrained by limited observations and required several pragmatic assumptions. Hydrometric records were only available at the Peam Khley station, so upstream inflows were model-derived, which limits the separation of rainfall uncertainty from runoff response. River channel geometry was surveyed at 12 representative sites; intervening reaches were interpolated from DEM-based indices, and Manning's roughness followed prior regional values by land cover, meaning small structures not explicitly represented may introduce local bias. Topography came from the MERIT DEM (90 m)

resampled to 500 m for consistency (Section 2.3), which smooths microtopography in urban or reclaimed areas and can underestimate shallow ponding.

Meteorological inputs (GSMaP) were bias-corrected with gauges using the RESTEC method (IDW approach) yet residual spatial errors can persist—especially for short, intense convective bursts. Validation relied on Sentinel-1 SAR; inundation under vegetation, urban layover/shadow or floating macrophytes may be undetected. For this event, Boeung Cheung Aek Lake was treated as inundated to account for macrophyte coverage. These assumptions were adopted to ensure stability and reproducibility under data-scarce conditions and are taken into account when interpreting the results in Section 4.

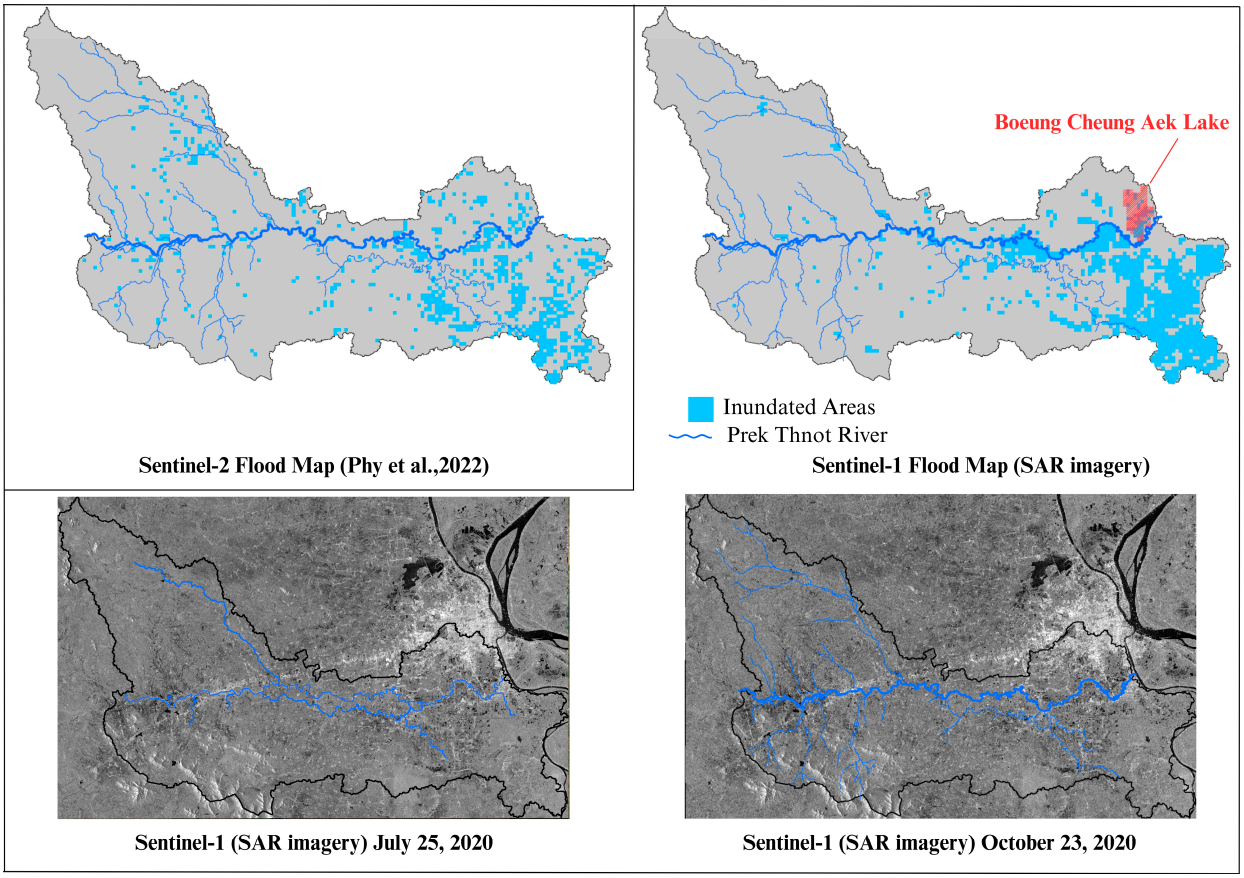


Figure 9. Flood extent in the 2020 flood over the Lower Prek Thnot River Basin detected by satellite imagery. Sentinel-2 flood map was adapted from Phy et al., (2022) [25].



Figure 10. Floating crop cultivation on Boeung Cheung Aek Lake.

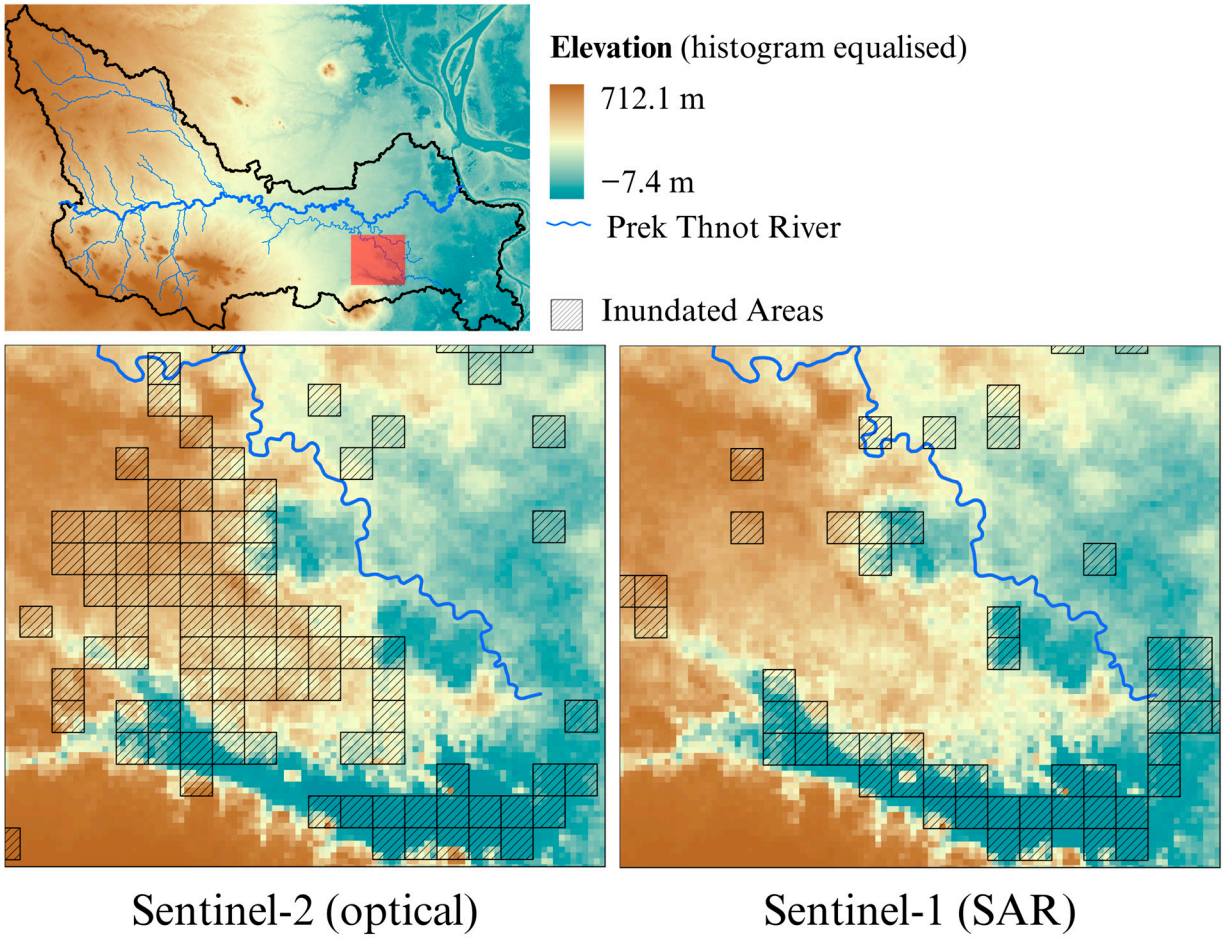


Figure 11. Comparison of inundated areas detected by Sentinel-2 (optical) and Sentinel-1 (SAR) imagery.

4. Results and Discussion

This section evaluates how the integration of satellite-derived datasets and field observations improved flood simulation performance in the LPTRB. The analysis follows the stepwise design introduced in Table 3, which summarises the data augmentation applied in each simulation (Sims. 0–5).

Table 3. Data augmentation and corresponding model performance.

	Data Augmentation			
Sim.	**Cross-Section**	**Hourly Rainfall**	**Land-Use**	**Infrastructure (Weir, Pump)**
0				
1	○			
2		○		
3	○	○		
4	○	○	○	
5	○	○	○	○

Note: ○ indicates that the corresponding data component is included in the simulation setting.

Each subsection below examines how augmenting the model with individual or combined data components—river channel cross-sections, hourly rainfall, land-use update and hydraulic infrastructure—affects model performance. To assess model performance, the area where the simulated inundation matched the SAR-derived flood map (referred to here as the "matched area") was calculated. In addition, three performance indices were

used: Accuracy (AC), Hit Ratio (HR) and True Ratio (TR) from Equations (9)–(11). In this study, a flood depth threshold of 0.4 m was set in the model, following a previous study conducted at a similar spatial scale [45].

$$AC = \frac{IC_{match} + UC_{match}}{TC} = \frac{IC_{obs} \cap IC_{sim} + UC_{obs} \cap UC_{sim}}{TC} \quad (9)$$

$$HR = \frac{IC_{match}}{IC_{obs}} = \frac{IC_{obs} \cap IC_{sim}}{IC_{obs}} \quad (10)$$

$$TR = \frac{IC_{match}}{IC_{sim}} = \frac{IC_{obs} \cap IC_{sim}}{IC_{sim}} \quad (11)$$

where IC, UC and TC are the number of inundated cells, un-inundated cells and total cells; and $IC_{match} (= IC_{obs} \cap IC_{sim})$ and UC_{match} $(= UC_{obs} \cap UC_{sim})$ are intersections between observed and simulated inundated and un-inundated cells.

4.1. Overall Performance Across Simulations

Sim. 0 serves as the baseline without any augmentation. Sims. 1 to 3 tested the effect of single or paired augmentations, specifically incorporating surveyed cross-sections, hourly rainfall input and their combination. Sims. 4 and 5 integrated multiple datasets simultaneously, including land-use and infrastructure. This stepwise approach allows assessment of the incremental contribution of each augmentation method to the accuracy and reliability of flood inundation modelling.

Figure 12 provides a spatial comparison between the simulated and observed flood extents for each scenario (Sim. 0–5). Blue, red and green grids represent the Sentinel-1-derived flood extent, simulated inundation and the matched area, respectively. Progressive improvement from Sim. 0 to Sim. 5 demonstrates the contribution of successive data augmentations to model performance.

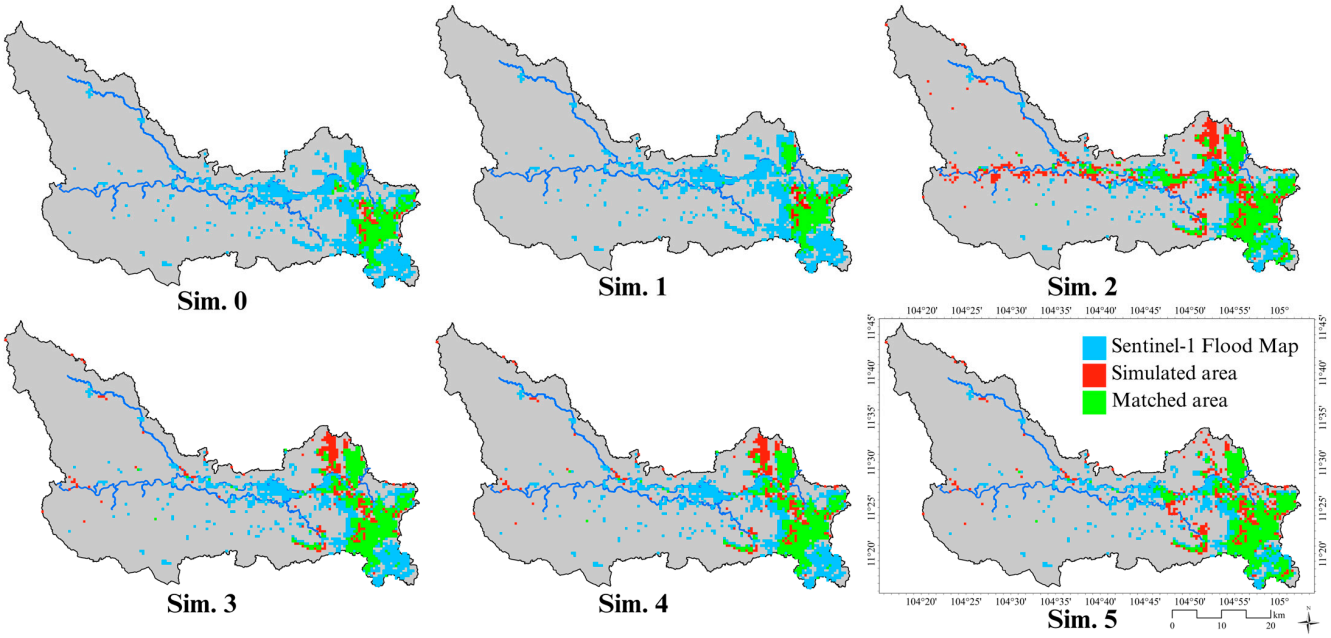


Figure 12. Spatial comparison of simulated flood extent with Sentinel-1 flood map.

The baseline case (Sim. 0), which relies solely on daily rainfall and default river geometry, reproduces flooding only in the lowermost portion of the basin. Sim. 1, incorporating field-surveyed cross-sections, shows a modest contraction of the inundated area as increased channel capacity conveys more flow downstream. Sim. 2, using hourly bias-

corrected rainfall, expands the flooded area substantially, capturing intense local rainfall events but also generating false inundation along upstream and middle reaches where default cross-sections remain undersized. Sim. 3 through Sim. 5 progressively refine the flood distribution, reducing false positives in Phnom Penh's city centre while improving correspondence with observed flood patterns near Boeung Cheung Aek Lake and other low-lying zones. Overall, these maps illustrate how data enrichment enhances spatial realism across the LPTRB. These visual improvements are quantitatively supported by the performance metrics shown below.

Following this spatial comparison, Figure 13 and Table 4 summarise the corresponding quantitative evaluation metrics—AC, HR and TR—together with the simulated and matched reas for each scenario. The baseline simulation (Sim. 0) achieves moderate accuracy (AC = 0.88) but relatively low HR, indicating that the model captured only part of the observed inundation. With the inclusion of higher-resolution rainfall and local hydraulic information, these indicators gradually improve, reaching the highest overall accuracy in Sim. 5 (AC = 0.891, HR = 0.546, TR = 0.701). This quantitative progression confirms the spatial patterns observed in Figure 12 and demonstrates that each step of data augmentation contributes to improved flood-extent representation. Sentinel-1 SAR data were used as the primary validation source owing to their robustness under cloudy monsoon conditions (see Section 3.5), providing a reliable benchmark for assessing simulation performance consistent with regional practices in Southeast Asia [43,44].

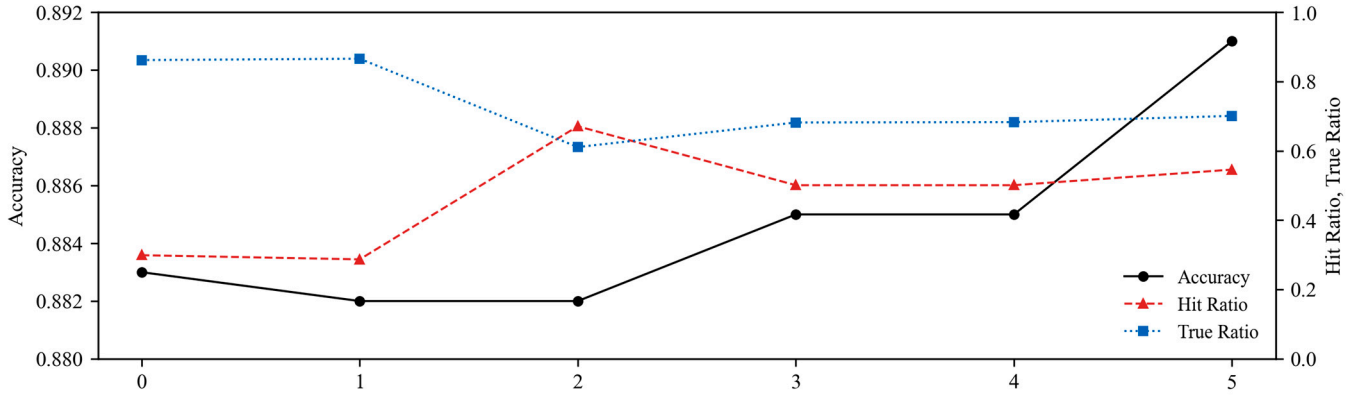


Figure 13. Comparison of model performance metrics: Accuracy, Hit Ratio and True Ratio across six simulations (Sim. 0–5).

Table 4. Simulated and matched areas, and corresponding performance metrics (Sim. 0–5).

Sim.	Simulated Area (km^2)	Matched Area (km^2)	AC	HR	TR
0	92.25	79.50	0.883	0.299	0.862
1	88.00	76.25	0.882	0.287	0.866
2	292.00	178.50	0.882	0.671	0.611
3	195.50	133.25	0.885	0.501	0.682
4	195.00	133.25	0.885	0.501	0.683
5	207.25	145.25	0.891	0.546	0.701

Note: Sentinel-1 derived estimated inundated area: 305.5 km^2

Compared with Sim. 0, corresponding to the results reported by Phy et al. (2022) [25], this study framework emphasises (a) explicit integration of surveyed river cross-sections, (b) incorporation of hourly GSMaP rainfall with gauge-based correction and (c) representation of hydraulic infrastructure such as pumps and weirs. While Phy et al. (2022) [25] focused on evaluating climate-induced discharge changes and flood susceptibility under daily rainfall forcing at the same spatial scales, our results suggest that surveyed geometry

and drainage operations are decisive for reproducing the spatial pattern of inundation during high monsoon flows.

When validated against different remote sensing datasets, performance metrics varied notably. Using Sentinel-2 as reference, the AC reached 0.896, which was higher than the 0.833 obtained with Sentinel-1. By contrast, the HR improved from 0.267 (Sentinel-2) to 0.299 (Sentinel-1), and the TR increased substantially from 0.423 (Sentinel-2) to 0.862 (Sentinel-1). The relatively high AC with Sentinel-2 can be explained by differences in the detected flood extent. Sentinel-2 identified a smaller inundated area (197.5 km^2) compared to Sentinel-1 (305.5 km^2). Since Sim. 0 reproduced flooding only in a limited part of the downstream reach, its simulated inundation extent was also small. Because AC is calculated using both inundated and non-inundated areas, the comparison between the smaller flood extent detected by Sentinel-2 and the similarly small extent simulated by the model resulted in an apparently higher AC value, despite the model's limited ability to capture actual inundation dynamics.

4.2. Combined Effects of Channel Geometry and Rainfall Resolution (Sims. 0–3)

The influence of both river channel representation and rainfall resolution was examined through Sims. 1–3, which progressively incorporated surveyed cross-sections, hourly bias-corrected rainfall and their combination. These experiments collectively assess how hydraulic structure and temporal rainfall detail interact to shape flood extent in the LPTRB.

The effect of incorporating actual river channel cross-section data was first assessed in Sim. 1, where only surveyed cross-sections were introduced while rainfall inputs remained uncorrected. In this case, the simulated inundation area decreased from 92.25 km^2 in Sim. 0 to 88.00 km^2. Consequently, AC slightly decreased from 0.883 to 0.882. This reduction in simulated flood extent can be attributed to differences in channel capacity between default and surveyed profiles. Field measurements revealed that the actual channels were wider and deeper upstream compared to the default, flow-accumulation-derived sections thereby increasing conveyance capacity and delaying overbank flow under identical rainfall forcing. This effect is clearly illustrated in the longitudinal water-level profiles along the main Prek Thnot River (Figure 14), where Sim. 1 exhibits lower water surfaces in the upper and middle reaches compared with Sim. 0. The reduction in simulated flood extent is therefore attributable to enhanced channel conveyance rather than changes in rainfall input. This finding highlights that geometric inaccuracies can mimic hydrological bias, producing overestimated flood extents even when rainfall inputs are accurate, consistent with prior RRI-based applications in low-gradient basins [23].

The replacement of daily rainfall with hourly GSMaP data via the RESTEC-IDW method (Section 3.1) was assessed in Sim. 2. It caused a sharp increase in the simulated inundation area (92.25 to 292.00 km^2). Although the HR improved to 0.671, the AC slightly decreased (0.883 to 0.882), reflecting a trade-off between detecting true floods and generating false positives. The hourly rainfall captured short-duration, high-intensity events that were previously smoothed out in daily totals; however, in the upper and middle reaches—where default cross-sections remained undersized—the model underestimated conveyance capacity and consequently overpredicted floodplain spreading (Figure 12). Thus, while temporal refinement of rainfall improves hydrologic realism, its benefits are conditional on physically plausible channel capacity, a crucial insight for flood modelling under data-scarce conditions.

The combined effect of hourly satellite rainfall input and surveyd cross-section data was evaluated in Sim. 3. When actual cross-sections were integrated with bias-corrected hourly rainfall, the model markedly improved overall its performance. The simulated inundation area decreased to 195.50 km^2, and the matched area reached 133.25 km^2. AC

improved to 0.885. These results demonstrate a clear complementarity: rainfall resolution governs when and how much water enters the system, while channel geometry determines where overflow occurs.

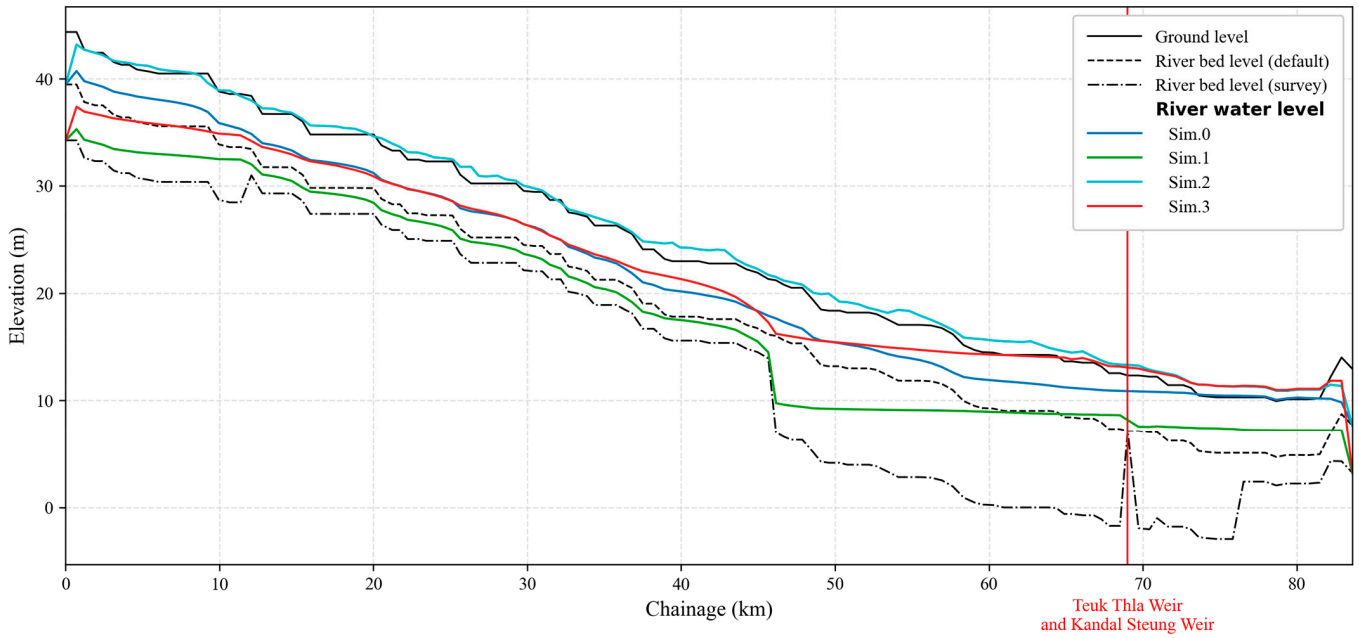


Figure 14. Longitudinal water level profiles along the main Prek Thnot River for Sim. 0 (default geometry), Sim. 1 (surveyed cross-sections) and Sim. 2–3 (hourly rainfall integration) at 00:00 on 23 October 2020.

Nevertheless, limitations remain. As shown in Figure 13, despite the increase in AC, the model still tended to overestimate flooding in central Phnom Penh and underrepresent inundation immediately upstream of the weirs, suggesting that local hydraulic controls—such as weir backwater and pumping operations—were not yet captured even after incorporating cross-sectional data. This pattern reinforces findings from previous urban studies that stormwater infrastructure and its operation, rather than land-surface change alone, critically shape inundation dynamics in rapidly urbanising areas [15,17,19].

4.3. Effect of Land Use Update (Sim. 3 to Sim. 4)

Updating the land-use dataset from 2002 to 2020 resulted in only minimal change in model performance. As described in Section 3.2, the land-use information was derived from Landsat-based global land cover products and reclassified into five categories—Forest, Urban, Agriculture, Water body, and Wetland—following the Mekong River Commission scheme. The original 30 m data were resampled to 500 m resolution using a majority filter to align with the RRI model grid, thereby preserving dominant land-cover patterns while suppressing speckle from mixed pixels.

A basin-wide comparison between 2002 and 2020 showed marked urban expansion (from 0.8% to 17.0%) and declines in agriculture and forest by about 10.5 and 6.9 percentage points, respectively, along with localised wetland loss in peri-urban areas (Figure 6). Despite these pronounced changes at the landscape scale, the 500 m aggregation inevitably smooths parcel-level heterogeneity in roughness and infiltration, limiting its impact on the distributed parameters used in the model.

The absence of clear improvement in flood simulation accuracy can therefore be explained by two factors. First, at the 500 m grid resolution, surface parameters such as Manning's coefficient and infiltration rate are averaged across mixed land-use pixels, muting the effect of fine-scale urbanisation. Second, for this extreme rainfall event, flood

extent is primarily governed by rainfall timing, boundary water levels, and hydraulic controls—particularly channel conveyance and drainage operations—rather than gradual surface-property changes. Although previous studies have documented strong associations between urban expansion and increased flood exposure in Phnom Penh [17–19], such land-use effects become evident only when both the spatial resolution and event magnitude are suited to capture them. This finding implies that, in mid-scale peri-urban basins such as the LPTRB, dynamic hydrometeorological forcing may overshadow land-cover influences on binary flood extent under extreme rainfall conditions.

4.4. Effect of Hydraulic Infrastructure (Sim. 4 to Sim. 5)

Sim. 5, the final and most comprehensive scenario, incorporated hydraulic infrastructure—namely the Teuk Thla and Kandal Steung weirs and the Tompun Pumping Station—alongside all prior data enhancements. This configuration yielded the best overall model performance, achieving the highest accuracy (AC = 0.891) among all scenarios. Flooding immediately upstream of the weirs, which had not been reproduced in earlier simulations, was successfully simulated, albeit with slightly underestimated extent. More importantly the model captured drainage reduction in central urban areas once pumping operations were emulated, reducing the excessive inundation seen in earlier simulations (Figure 13). The results demonstrate that accurate representation of flow regulation and pumping operations is essential for simulating intra-urban flood behaviour, echoing the institutional analyses that identified inadequate drainage as a key source of vulnerability in Phnom Penh [20–22]. Therefore, Sim. 5 provides a quantitative response to one of the study's core research questions: operational infrastructure exerts first-order control over flood distribution in peri-urban Phnom Penh, surpassing the influence of land-cover change alone.

4.5. Practical Implications, Limitations, and Synthesis

Spatial comparison between simulated and observed flood maps revealed consistent error patterns and clarified the relative importance of different controlling factors. Overestimation in the upper and middle reaches (Sim. 2) was mainly caused by undersized default channel geometry, which was largely corrected once the surveyed cross-sections were introduced (Sim. 3 onward). Excessive inundation in central Phnom Penh, linked to drainage bottlenecks, was effectively mitigated only after incorporating pumping operations in Sim. 5. Wetland complexes such as Boeung Cheung Aek and Boeung Cheung Loung acted as natural retention basins, confirming their crucial role in attenuating peak runoff and underscoring the importance of wetland preservation—consistent with previous findings on land transformation and flood susceptibility in Phnom Penh [17–19].

The incremental simulations collectively highlight a hierarchy of controlling factors governing model performance: (1) rainfall resolution and bias correction determine the timing and magnitude of flood generation; (2) channel geometry governs spatial routing and overflow locations; (3) hydraulic infrastructure operations redistribute floodwater and control drainage recovery; and (4) land-use change exerts only a secondary influence at the 500 m modelling scale. This hierarchy provides a practical roadmap for improving flood modelling under data-scarce conditions—refine rainfall and geometry first, incorporate infrastructure operations next, and update land-use representation as resolution permits. Finally, comparison with Sentinel-2 imagery confirmed that its smaller detected flood extent leads to inflated accuracy (AC), reaffirming the need to interpret AC jointly with HR and TR for robust validation.

5. Conclusions

This study demonstrated that flood inundation modelling in the Lower Prek Thnot River Basin can be substantially improved through data augmentation that includes bias-corrected hourly satellite rainfall, field-surveyed river channel cross-sections and hydraulic infrastructure such as weirs and pumping stations. The enhanced configuration (Sim. 5) achieved the highest performance (AC = 0.891) in reproducing the October 2020 flood event, demonstrating the effectiveness of combining remotely sensed and locally observed data for hydrodynamic flood simulation in data-scarce environments. The results clarified the relative influence of individual data components. Rainfall resolution and bias correction controlled the timing and magnitude of flooding, while observed channel geometry governed spatial routing and overflow locations. Hydraulic infrastructure operations—pumping and gate control—were found to be decisive for simulating drainage and recovery processes, whereas land-use updates exerted only minor influence at the 500 m resolution. These findings further confirmed that rainfall input and channel geometry are closely related: neither rainfall input nor channel geometry alone improved accuracy, but inclusion of both factors yielded a more accurate representation of actual inundation patterns. Data scarcity is not confined to Cambodia or Southeast Asia, but remains a global challenge that continues to concern scientists, policy-makers and practitioners alike. In river basins with limited observational data, the integration of bias-corrected satellite rainfall data and surveyed channel geometry is therefore recommended as a practical means of enhancing model reliability.

Beyond methodological advancement, the findings offer practical implications for flood management in Phnom Penh's rapidly urbanising areas. Natural wetlands such as Boeung Cheung Aek and Boeung Cheung Loung were identified as critical retention zones that attenuate flood peaks, while proper documentation and management of drainage infrastructure operations were shown to strongly affect inundation extent. These insights support the adoption of nature-based retention and adaptive infrastructure operation as effective strategies for mitigating flood risk in expanding urban areas.

One caveat of this study is the limited availability of flood depth records for model validation. Enhanced systematic field data collection during flood events may help overcome this limitation and improve the reliability of future modelling.

Author Contributions: Conceptualization, Y.I. and T.K. (Takuto Kumagae); methodology, Y.I. and T.K. (Takuto Kumagae); software, H.A. and T.K. (Takuto Kumagae); validation, T.K. (Takuto Kumagae); formal analysis, Y.I. and T.K. (Takuto Kumagae); investigation, T.K. (Takuto Kumagae), H.A. and M.N.; data curation, T.K. (Takuto Kumagae); writing—original draft preparation, T.K. (Takuto Kumagae) and M.N.; writing—review and editing, T.K. (Toru Konishi) and Y.I.; supervision, Y.I.; project administration, Y.I.; funding acquisition, Y.I. All authors have read and agreed to the published version of the manuscript.

Funding: This research was funded by Tokyo Human Resources Fund for City Diplomacy.

Data Availability Statement: Publicly available datasets were analysed in this study. GSMaP_MVK (ver. 7.3112.0), satellite rainfall data are available from the JAXA GLOBAL RAINFALL WATCH https://sharaku.eorc.jaxa.jp/GSMaP/ (accessed on 26 November 2024). Sentinel-1 imagery can be obtained through the Google Earth Engine https://earthengine.google.com/. The MERIT DEM is open access at the University of Tokyo MERIT DEM website https://hydro.iis.u-tokyo.ac.jp/~yamadai/MERIT_DEM/ (accessed on 10 December 2024). The Rainfall–Runoff–Inundation (RRI) model (version 1.4.2) is freely available from the ICHARM https://www.pwri.go.jp/icharm/research/rri/rri_top.html (accessed on 17 June 2024). Hydrological data such as rainfall gauges, water level and discharge were provided by the Ministry of Water Resources and Meteorology (MOWRAM), Cambodia, and are available from the corresponding author upon reasonable request with the permission of MOWRAM.

The datasets presented in this article are not readily available because the data are part of an ongoing study. Requests to access the datasets should be directed to the corresponding author.

Acknowledgments: We gratefully acknowledge the Department of Hydrology and River Works, Ministry of Water Resources and Meteorology (MOWRAM), Cambodia, for providing the rainfall data used in this study. We also thank Ty Sok, Ilan Ich, and Sophea Rom Phy for providing hydrological data, including data of the Prek Thnot River Basin, Mekong flood extent maps and flood simulation results from the RRI model. We are grateful to Shun Kudo (Public Works Research Institute), Mamoru Miyamoto and Naoko Nagumo (International Centre for Water Hazard and Risk Management) for their technical and conceptual advice.

Conflicts of Interest: The authors declare no conflicts of interest.

Abbreviations

The following abbreviations are used in this manuscript:

LPTRB	Lower Prek Thnot River Basin
MOWRAM	Ministry of Water Resources and Meteorology
RRI	Rainfall-Runoff Inundation
JICA	Japan International Cooperation Agency
DEM	Digital Elevation Model
DIR	Flow Direction
ACC	Flow Accumulation
GSMaP	Global Satellite Mapping of Precipitation
SAR	Synthetic Aperture Radar
AC	Accuracy
HR	Hit Ratio
TR	True Ratio
IC	Inundated cells
UC	Un-inundated cells
TC	Total cells

References

1. UNDRR Human Cost of Disasters. UNDRR. Geneva, CHE. 2000. Available online: https://www.undrr.org/media/48008/download?startDownload=20250715 (accessed on 14 August 2025).
2. IPCC. *Climate Change 2023: Synthesis Report. Contribution of Working Groups I, II and III to the Sixth Assessment Report of the Intergovernmental Panel on Climate Change*; Core Writing Team, Lee, H., Romero, J., Eds.; IPCC: Geneva, Switzerland, 2023; pp. 35–115. [CrossRef]
3. Iwami, T.; Hasegawa, T.; Miyamoto, M.; Kudo, S.; Yamazaki, Y.; Ushiyama, T.; Koike, T. Comparative study on climate change impact on precipitation and floods in Asian river basins. *Hydrol. Res. Lett.* **2017**, *11*, 24–30. [CrossRef]
4. Shrestha, B.B.; Perera, E.D.P.; Kudo, S.; Miyamoto, M.; Yamazaki, Y.; Kuribayashi, D.; Sawano, H.; Sayama, T.; Magome, J.; Hasegawa, A.; et al. Assessing flood disaster impacts in agriculture under climate change in the river basins of Southeast Asia. *Nat. Hazard.* **2019**, *97*, 157–192. [CrossRef]
5. IPCC. *Climate Change 2021: The Physical Science Basis. Contribution of Working Group I to the Sixth Assessment Report of the Intergovernmental Panel on Climate Change*; Cambridge University Press: Cambridge, UK, 2021. [CrossRef]
6. UNDESA. *World Population Prospects 2019: Highlights*; United Nations, Department of Economic and Social Affairs, Population Division: New York, NY, USA, 2019. Available online: https://population.un.org/wpp/assets/Files/WPP2019_Highlights.pdf (accessed on 1 September 2025).
7. ADB. *Asian Water Development Outlook 2020: Advancing Water Security Across Asia and the Pacific*; Asian Development Bank: Mandaluyong City, Philippines, 2020. [CrossRef]
8. Sayama, T.; Tatebe, Y.; Iwami, Y.; Tanaka, S. Hydrologic sensitivity of flood runoff and inundation: 2011 Thailand floods in the Chao Phraya River basin. *Nat. Hazards Earth Syst. Sci.* **2015**, *15*, 1617–1630. [CrossRef]
9. Shakti, P.C.; Miyamoto, M.; Misumi, R.; Nakamura, Y.; Sriariyawat, A.; Visessri, S.; Kakinuma, D. Assessing flood risk of the Chao Phraya River Basin based on statistical rainfall analysis. *J. Disaster Res.* **2020**, *15*, 1025–1039. [CrossRef]
10. Jamrussri, S.; Toda, Y. Assessing the effectiveness of non-structural flood countermeasures in the upper Chao Phraya River Basin, Thailand. *J. Hydrol. Reg. Stud.* **2017**, *10*, 82–94. [CrossRef]

11. Koem, C.; Tantanee, S. Flood Disaster Studies: A Review of Remote Sensing Perspective in Cambodia. *Geogr. Tech.* **2021**, *16*, 13–24. [CrossRef]
12. Phy, S.R.; Sok, T.; Try, S.; Chan, R.; Uk, S.; Hen, C.; Oeurng, C. Flood Hazard and Management in Cambodia: A Review of Activities, Knowledge Gaps, and Research Direction. *Climate* **2022**, *10*, 162. [CrossRef]
13. Horton, A.J.; Triet, N.V.K.; Hoang, L.P.; Heng, S.; Hok, P.; Chung, S.; Koponen, J.; Kummu, M. The Cambodian Mekong floodplain under future development plans and climate change. *Nat. Hazards Earth Syst. Sci.* **2022**, *22*, 967–983. [CrossRef]
14. Vichet, N.; Kawamura, K.; Trong, D.P.; On, N.V.; Gong, Z.; Lim, J.; Khom, S.; Bunly, C. MODIS-Based Investigation of Flood Areas in Southern Cambodia from 2002–2013. *Environments* **2019**, *6*, 57. [CrossRef]
15. Huang, W.; Park, E.; Wang, J.; Sophal, T. The changing rainfall patterns drive the growing flood occurrence in Phnom Penh, Cambodia. *J. Hydrol. Reg. Stud.* **2024**, *55*, 101945. [CrossRef]
16. Tierolf, L.; Moel, H.D.; Vliet, J.V. Modeling urban development and its exposure to river flood risk in Southeast Asia. *Comput. Environ. Urban Syst.* **2021**, *87*, 101620. [CrossRef]
17. Mialhe, F.; Gunnell, Y.; Navratil, O.; Choi, D.; Sovann, C.; Lejot, J.; Gaudou, B.; Se, B.; Landon, N. Spatial growth of Phnom Penh, Cambodia (1973–2015): Patterns, rates, and socio-ecological consequences. *Land Use Policy* **2019**, *87*, 104061. [CrossRef]
18. Son, T.N.; Thi Thu Trang, N.; Bui, X.T.; Thi Da, C. Remote sensing and GIS for urbanization and flood risk assessment in Phnom Penh, Cambodia. *Geocarto Int.* **2022**, *37*, 6625–6642. [CrossRef]
19. Khan, L. An economic assessment of urban flooding in Cambodia: A case study of Phnom Penh. *Insight Cambodia J. Basic Appl.* **2019**, *1*, 125–149. [CrossRef]
20. Sahmakum Teang Tnaut (STT). Poverty Assessment for Urban Poor Communities in Phnom Penh. 2022. Available online: https://teangtnaut.org/en/research/reports/poverty-assessment-for-urban-poor-communities-in-phnom-penh (accessed on 22 September 2025).
21. Nop, S.; Thornton, A. Urban resilience building in modern development. *Ecol. Soc.* **2019**, *24*, 23. [CrossRef]
22. Flower, B.; Fortnam, M. Urbanising Disaster Risk: Vulnerability of the Urban Poor in Cambodia to Flooding and Other Hazards. 2015. Available online: https://www.preventionweb.net/files/submissions/47109_urbanisingdisasterriskreportinteractive.pdf (accessed on 22 August 2025).
23. Kudo, S.; Yorozuya, A.; Perera, E.D.P.; Koseki, H.; Iwami, Y.; Nakatsugawa, M. Influence Analysis of Observed River Channel Conditions of Inundation Process in Lower Mekong River Basin. *Jpn. J. JSCE* **2016**, *72*, 145–150. (In Japanese) [CrossRef] [PubMed]
24. Heng, S.; Kheav, K.; Hok, P.; Chhuon, K.; Ly, S.; Kinouchi, T. Urban Flood Modeling in Phnom Penh Using Flo-2D: Consideration of Climate Change Effect. *Techno-Sci. Res. J.* **2021**, *9*, 33–40.
25. Phy, S.R.; Try, S.; Sok, T.; Ich, I.; Chan, R.; Oeurng, C. Integration of Hydrological and Flood Inundation Models for Assessing Flood Events in the Lower Prek Thnot River Basin under Climate Change. *J. Hydrol. Eng.* **2022**, *27*, 05022012. [CrossRef]
26. Srey, S.; Yaguchi, T. The Peri-Urban Landscape Interface Contribution to Flood Management of The Metropolis, The Case of Phnom Penh. Journal of Architecture Planning. *Archit. Inst. Jpn.* **2023**, *88*, 1648–1659. [CrossRef]
27. The World Bank. Climate Change Knowledge Portal. 2024. Available online: https://climateknowledgeportal.worldbank.org/country/cambodia (accessed on 14 October 2025).
28. Ministry of Planning (MOP). *Commune Database: 2005–2022*; Unpublished Excel Data Set; Ministry of Planning (MOP) Commune Database: Phnom Penh, Cambodia, 2025.
29. OCIC Group. Techo International Airport. *OCIC Homepage.* 2023. Available online: https://www.ocic.com.kh/projects/techo-international-airport (accessed on 15 July 2025).
30. Raksmey, H. Techo International Airport: Cambodia's Emerging Passenger and Cargo Hub. The Phnom Post. 2025. Available online: https://www.phnompenhpost.com/national/techo-international-airport-cambodia-s-emerging-passenger-and-cargo-hub (accessed on 15 July 2025).
31. The World Bank Cambodia Country Office. *Urban Development in Phnom Penh Land Use Policy*; World Bank Group: Washington, DC, USA, 2017; Volume 87. Available online: https://documents.worldbank.org/en/publication/documents-reports/documentdetail/286991511862455372 (accessed on 22 August 2025).
32. Sayama, T.; Ozawa, G.; Kawakami, T.; Nabesaka, S.; Fukami, K. Rainfall-Runoff-Inundation Analysis of the 2010 Pakistan Flood in the Kabul River Basin. *Hydrol. Sci. J.* **2012**, *57*, 298–312. [CrossRef]
33. Kakinuma, D. 2022 PWRI New Technology Seminar in Tokyo. PWRI Homepage. 2022. Available online: https://www.pwri.go.jp/jpn/results/tec-info/siryou/seminar/R4/pdf/2022seminar_1555.pdf (accessed on 15 July 2025). (In Japanese).
34. Yamazaki, D.; Watanabe, S.; Hirabayashi, Y. Global Flood Risk Modeling and Projections of Climate Change Impacts. *Geophys. Monogr. Ser. Ch.* **2018**, *11*, 158–203. [CrossRef]
35. Cambodia Humanitarian Response Forum. Floods in Cambodia: Situation Report No. 6—Humanitarian Response Forum, As of 26 October 2020. KHM. 2020. Available online: https://reliefweb.int/report/cambodia/floods-cambodia-situation-report-no-6-humanitarian-response-forum-26-october-2020 (accessed on 23 December 2024).

36. Kamimera, H.; Thanh, N.D.; Le, V.X.; Matsumoto, J.; Ushio, T.; Iwami, Y. Evaluation of the performance of the satellite precipitation product GSMaP in central Vietnam. In Proceedings of the Japan Society of Hydrology and Water Resources Annual Conference 2014, Miyazaki, Japan, 26 September 2014; Volume 27, p. 100034. (In Japanese). [CrossRef]
37. Tsuda, M.; Application of Corrected GSMaP to flood Forecasting and Warning. JAXA Homepage. 2016. Available online: https://www.eorc.jaxa.jp/event/2016/pdf/06_tsuda.pdf (accessed on 15 July 2025). (In Japanese).
38. Potapov, P.; Hansen, M.C.; Pickens, A.; Hernandez-Serna, A.; Tyukavina, A.; Turubanova, S.; Zalles, V.; Li, X.; Khan, A.; Stolle, F.; et al. The Global 2000-2020 Land Cover and Land Use Change Dataset Derived from the Landsat Archive: First Results. *Front. Remote Sens.* **2022**, *3*, 856903. [CrossRef]
39. Wulder, M.A.; Masek, J.G.; Cohen, W.B.; Loveland, T.R.; Woodcock, C.E. Opening the Archive: How Free Data Has Enabled the Science and Monitoring Promise of Landsat. *Remote Sens. Environ.* **2012**, *122*, 2–10. [CrossRef]
40. Japan International Cooperation Agency. *The Study on Comprehensive Agricultural Development of Prek Thnot River Basin in The Kingdom of Cambodia*; Report; JICA: Tokyo, Japan, 2008.
41. Japan International Cooperation Agency. *Project for The Comprehensive Flood Management Plan for The Chao Phraya River Basin Final Report Addendum Report: The Flood Analysis on the Chao Phraya River with RRI Model*; Report; JICA: Tokyo, Japan, 2013.
42. Obata, S.; Shimatani, Y.; Sato, T. Evaluation of Flood Control Function of Irrigation Ponds in The Rokkaku River Watershed. *J. Jpn. Soc. Civ. Eng. Ser. B1* **2020**, *76*, 757–762. (In Japanese) [CrossRef] [PubMed]
43. Iida, Y.; Watanabe, N.; Sato, J.; Koarai, M. Disaster Monitoring using High Resolution SAR. *J. Geospat. Inf. Auth. Jpn.* **2002**, *99*, 49–56. Available online: https://gbank.gsj.jp/ld/resource/geolis/200211961 (accessed on 11 June 2024). (In Japanese).
44. Quang, N.H.; Tuan, V.A.; Hang, L.T.; Hung, N.M.; The, D.T.; Dieu, T.D.; Anh, N.D.; Hackney, C.R. Hydrological/Hydraulic Modeling-Based Thresholding of Multi SAR Remote Sensing Data for Flood Monitoring in Regions of the Vietnamese Lower Mekong River Basin. *Water* **2020**, *12*, 71. [CrossRef]
45. Yamamoto, K.; Sayama, T. Impact of climate change on flood inundation in a tropical river basin in Indonesia. *Prog. Earth Planet Sci.* **2021**, *8*, 5. [CrossRef]

Disclaimer/Publisher's Note: The statements, opinions and data contained in all publications are solely those of the individual author(s) and contributor(s) and not of MDPI and/or the editor(s). MDPI and/or the editor(s) disclaim responsibility for any injury to people or property resulting from any ideas, methods, instructions or products referred to in the content.